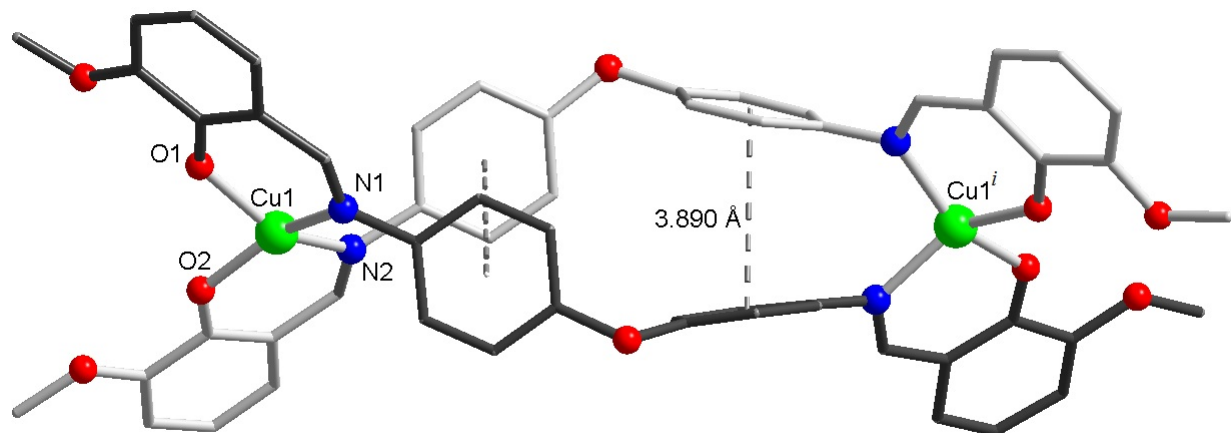


## Supporting Information

### Magnetic and luminescent binuclear double stranded helicates

Paula Cucos<sup>†</sup>, Floriana Tuna<sup>§</sup>, Lorenzo Sorace<sup>¶</sup>, Iulia Matei<sup>#</sup>, Catalin Maxim<sup>†</sup>, Sergiu Shova<sup>‡</sup>, Ruxandra Gheorghe<sup>†</sup>, Andrea Caneschi<sup>¶</sup>, Mihaela Hillebrand<sup>#</sup>, Marius Andruh<sup>†</sup>

## FIGURES



**Figure S1.** Representation of the intramolecular  $\pi$ - $\pi$  stacking for helicate **2** (centroid-centroid distance is given)

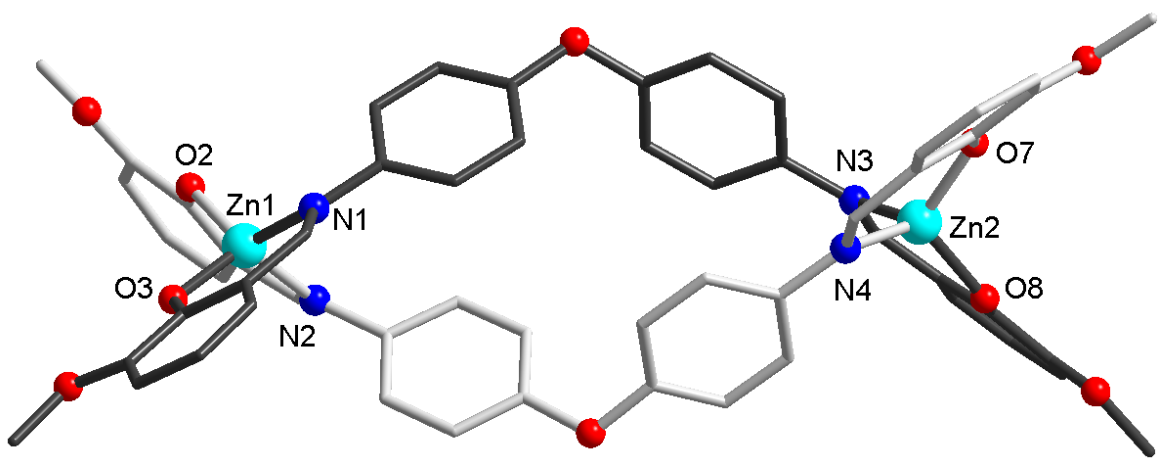


**Figure S2.** The molecular structure of the zinc helicate 3

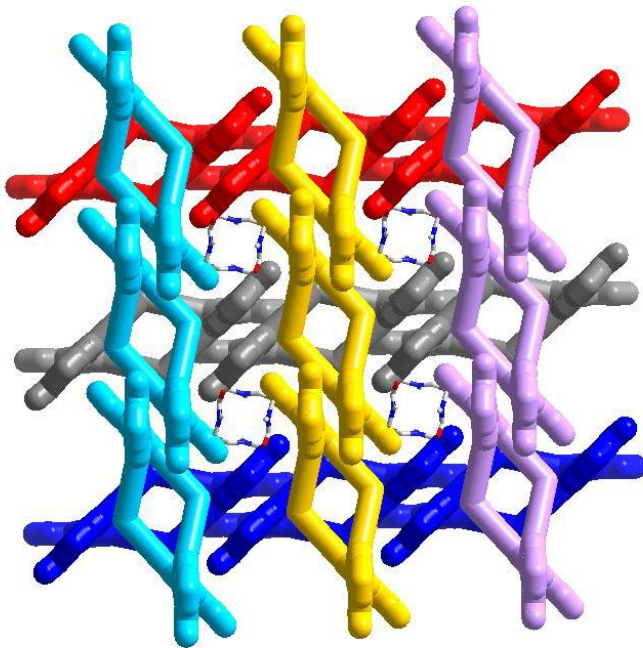


**Figure S3.** Detail of the packing diagram of the helicate 2 showing the formation of channels with included DMF molecules (supramolecular chains are differentiated by color).

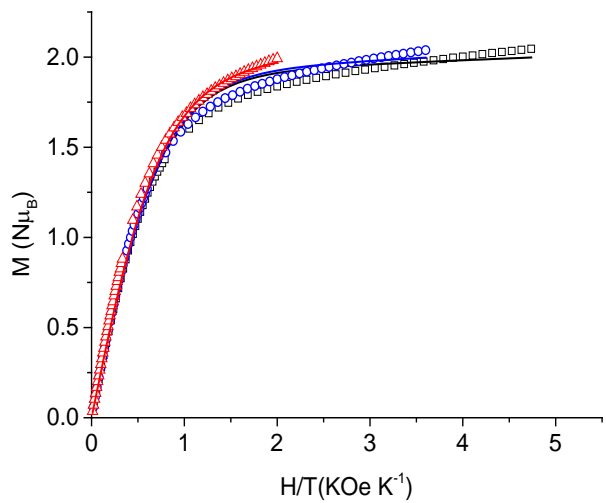


**Figure S4.** Best fit (continuous lines) of experimental isothermal magnetization curves, plotted as reduced magnetization measured at 1.9 (squares), 2.5 (circles) and 4.5 K (triangles), forcing  $D > 0$ . The much worse quality compared to the  $D < 0$  case reported in main text is evident.

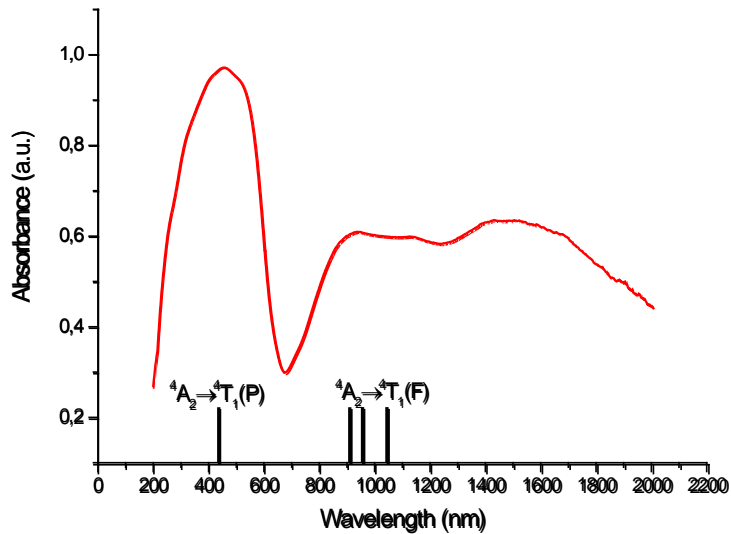
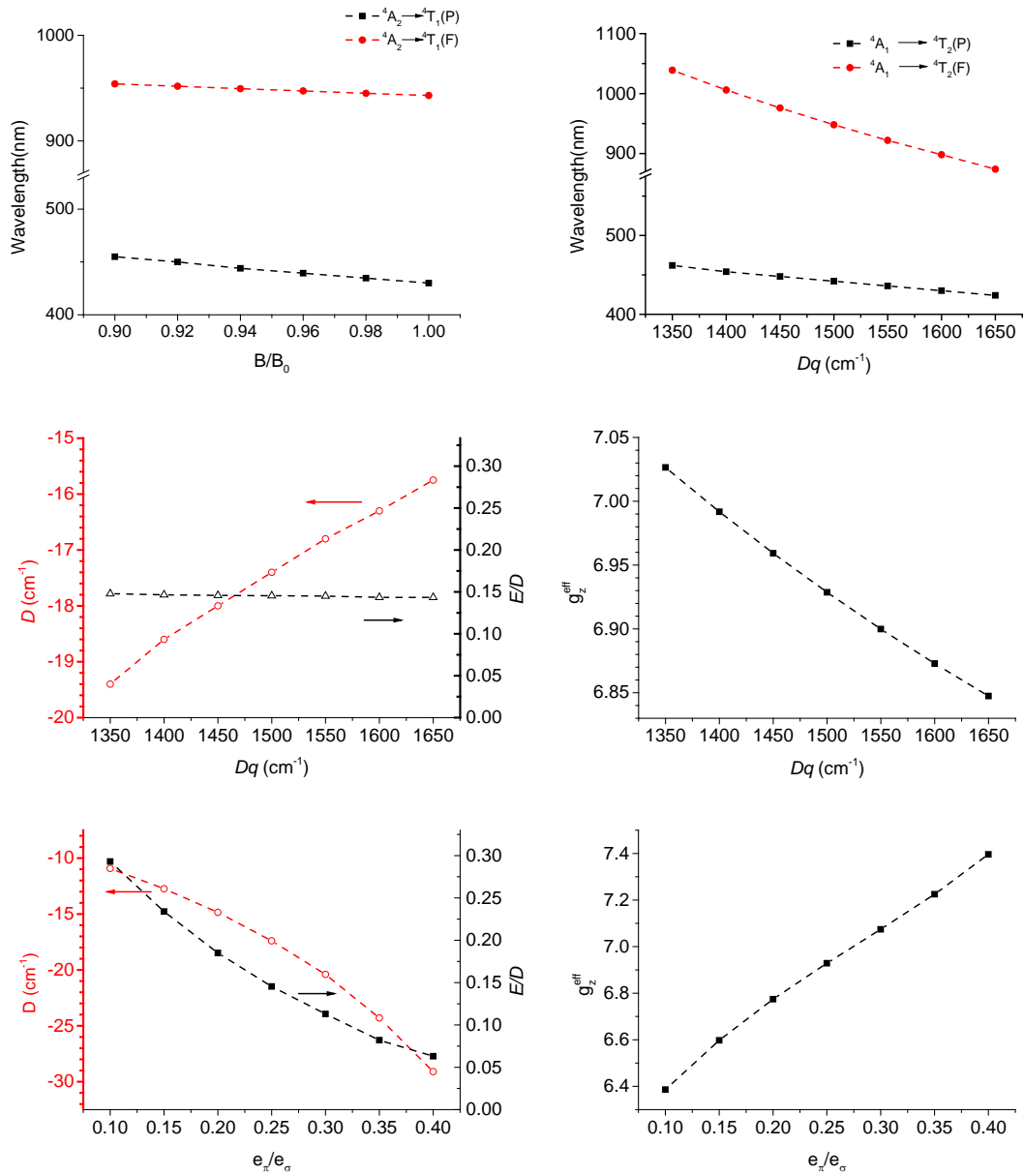


**Figure S5.** Diffuse reflectance spectrum for complex **1**. The sticks evidence the transition energies calculated by the AOM approach using the parameters reported in Table S1.



**Figures S6.** (upper): dependence of AOM calculated wavelength of the electronic transitions on  $B$  and  $Dq$ . (center): dependence of the  $D$ ,  $E/D$  and  $g_z^{\text{eff}}$  calculated by AOM on  $Dq$ . (lower): dependence of the  $D$ ,  $E/D$  and  $g_z^{\text{eff}}$  calculated by AOM on the  $e_\pi/e_\sigma$  ratio. Except when the corresponding parameter is varied, calculations were performed with the following set:  $B/B_0 = 0.95$ ;  $C = 3700 \text{ cm}^{-1}$ ,  $Dq = 1500 \text{ cm}^{-1}$ ,  $e_\pi/e_\sigma = 0.25$ ,  $e_{\pi c}(N)/e_{\pi s}(N) = 0$ ,  $e_{\pi c}(O)/e_{\pi s}(O) = 1$

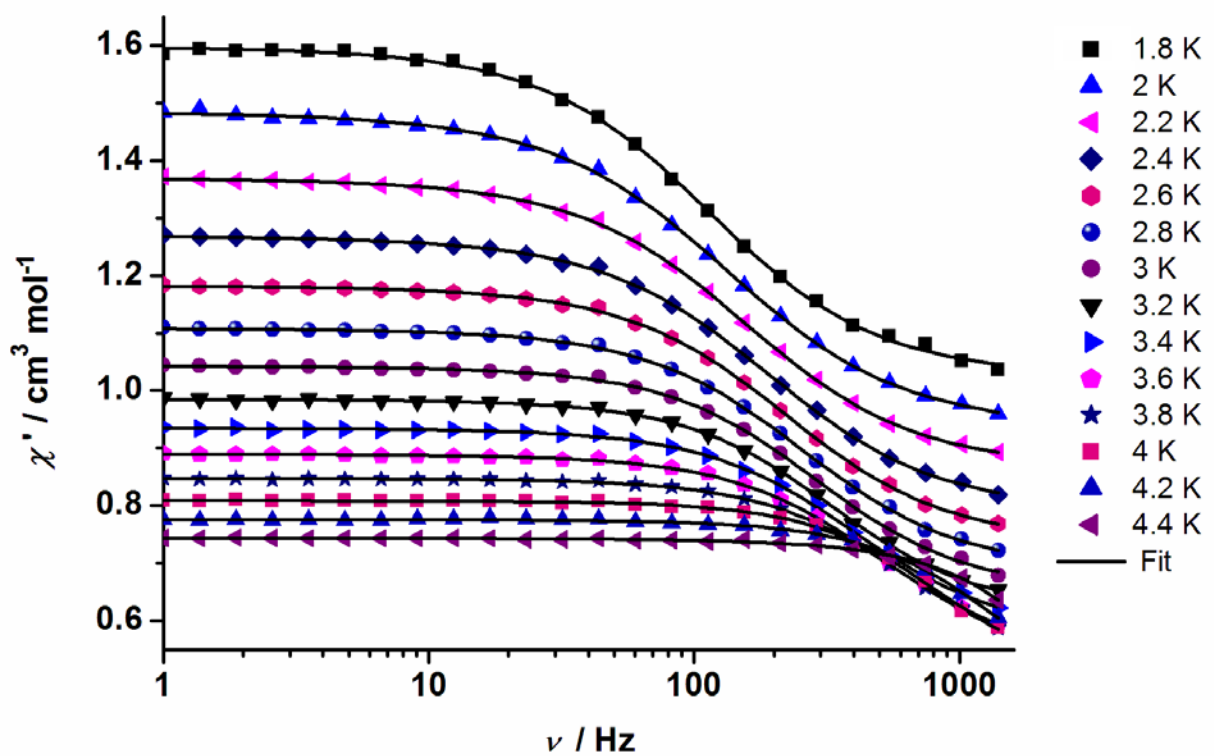


**Figure S7.** Frequency dependence of the in-phase ac susceptibility ( $\chi'$ ) of **1**

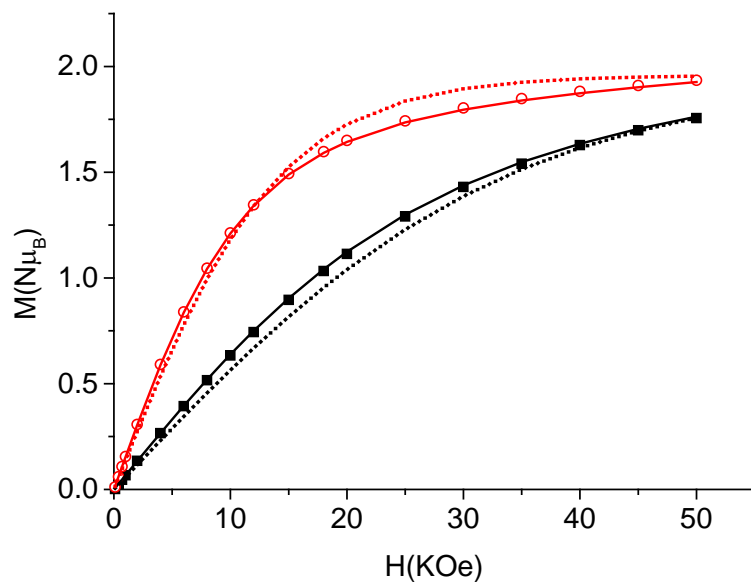


**Figure S8.** Isothermal magnetization, reported per effective number of Co(II) ion, measured at 1.9 (circles) and 4.5 K (squares) for  $\text{Zn}_{0.98}\text{Co}_{0.02}$ . Continuous lines represent the best fit obtained considering an easy axis anisotropy and parameters reported in the text. Dotted lines represent the best fit obtained considering an hard axis type anisotropy.

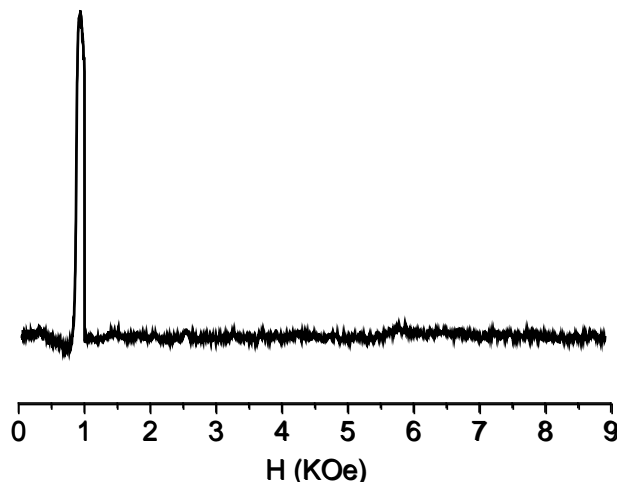


**Figure S9.** X-band (9.408 GHz) EPR spectrum of a microcrystalline powder sample of  $\text{Zn}_{0.98}\text{Co}_{0.02}$  measured at 5 K.

**Table S1.** Best parameter set for AOM calculation on **1**

Parameter	Value (cm <sup>-1</sup> )
$B$	910
$C$	3700
$\zeta$	-516
$K$	0.9
$e_{\sigma}$ (N,O)	6040
$e_{\pi s}$ (N)	1810
$e_{\pi c}$ (N)	0
$e_{\pi s,c}$ (O)	905